A simplified model of flexible power point tracking algorithms in double-stage photovoltaic systems

Candelaria Utrilla, Hossein Dehghani Tafti, Anusha Kumaresan, Jérôme Buire, Vincent Debusschere, Josep Pou, Nouredine Hadjsaid

A simplified model of flexible power point tracking algorithms in double-stage photovoltaic systems

Candelaria Utrilla[a], Hossein Dehghani Tafti[b], Anusha Kumaresan[c], Jérôme Buire[a], Vincent Debusschere[a,*], Josep Pou[d], Nouredine Hadjsaid[a,d]

[a] *Univ. Grenoble Alpes, CNRS, Grenoble INP, G2ELab, Grenoble, 38000, France*
[b] *Department of Electrical, Electronic and Computer Engineering, University of Western Australia, Crawley WA, 6009, Australia*
[c] *Energy Research Institute at NTU (ERI@N), Interdisciplinary Graduate Programme, Nanyang Technological University, Singapore, 639798, Singapore*
[d] *School of Electrical and Electronic Engineering, Nanyang Technological University, Singapore639798, Singapore*

Abstract

Traditionally, photovoltaic (PV) systems have been operated using maximum power point tracking algorithms, which force the PV arrays to produce the maximum available power at all times. Nevertheless, distribution system operators are increasingly asking for flexible power point tracking (FPPT) algorithms, which allow the regulation of the PV power to a predefined reference value. FPPTs are difficult to tune and often have non-linear behavior. It complicates the modeling of PV systems for power system stability studies. This paper proposes a simplified model that reproduces the dc-side dynamics of a double-stage FPPT-controlled PV system. In addition to its simple tuning, the key advantage of the proposed model is that it can be easily translated into differential equations, which can be used in stability analyses. The proposed model is validated on a temporal simulation as well as a small-signal stability study.

Keywords: Flexible power point tracking; Double-stage converter; Photovoltaic system; Modeling and control

1. Introduction

During the past decades, electrical grids have experienced an increased penetration of photovoltaic (PV) systems. The inverters of these systems are typically operated in grid-feeding mode, while the dc-side operation is governed by maximum power point tracking (MPPT) algorithms. These algorithms ensure that the PV arrays are continuously working at the operation point that delivers the maximum available power. However, distribution system operators are increasingly demanding a more flexible operation of grid-feeding PV systems. For instance, several grid codes already ask for these systems to implement power limiting control [1,2,6]. Furthermore, multiple works are investigating the grid-forming control of PV systems [4,8–11]. Both cases require substituting the MPPTs with other algorithms allowing them to regulate the PV arrays' output power to a predefined power reference. To this end, multiple flexible power point tracking (FPPT) algorithms have been proposed in the literature [13,15,17].

* Corresponding author.
E-mail address: vincent.debusschere@grenoble-inp.fr (V. Debusschere).

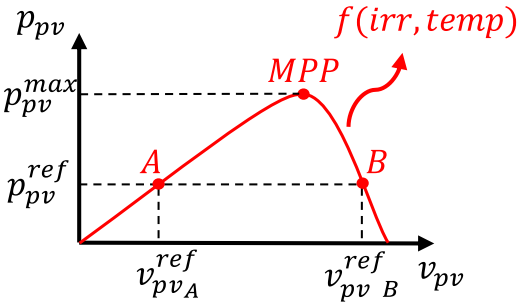

Fig. 1. The power-voltage characteristic curve of a PV array.

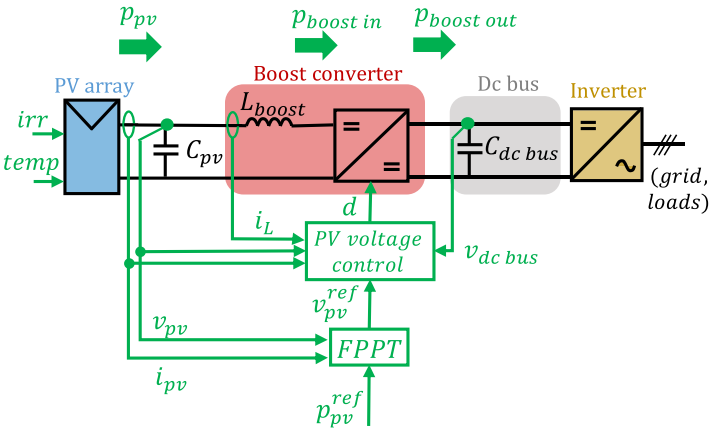

Fig. 2. Overview of a typical FPPT control in a double-stage PV system.

Fig. 1 depicts the typical power-voltage characteristic of a PV array, which is a function of the irradiation (irr) and the PV cells temperature ($temp$). The voltage at the PV array terminals is denoted as v_{pv} and p_{pv} is the power produced by the PV array. While MPPTs always force the system to operate at the maximum power point (MPP), FPPTs allow setting a variable power reference (p_{pv}^{ref}). It is important to note that two possible operating points lead to the same value of p_{pv} (point A and point B). Accordingly, some FPPTs only allow the system to operate on one side of the MPP, while others allow operation on both sides. Fig. 2 shows how an FPPT is normally inserted in the dc-side control of a double-stage PV system. A PV power reference is given to the FPPT, which calculates the voltage that should be imposed on the PV array's terminals to obtain the required power. Finally, this PV voltage reference (v_{pv}^{ref}) is sent to a control block that, by commanding the boost converter, makes v_{pv} converge towards its reference.

A key challenge of FPPT-controlled PV systems is that the dc-side control is not easy to design. Many FPPT algorithms have a large number of parameters and require a fine tuning to achieve appropriate performances, such as [13] or [18]. Furthermore, designing the PV voltage control is not a straightforward task either. Because of FPPT operation, the operating point of a PV array can widely vary and, in consequence, its dynamic response can considerably change [3]. In fact, advanced controllers (e.g., adaptive, predictive or nonlinear [12]) have been proposed to overcome this issue. These are important obstacles for researchers that focus on ac-side issues and that cannot afford to implement detailed models of the PV systems' dc side. In addition, these detailed models can often not be directly introduced in stability analyses, because of the nonlinear nature of the PV voltage control and/or of the FPPT (often based on decision trees).

In light of these facts, this paper proposes a simplified model for the dc side of a double-stage FPPT-controlled PV system. This model aims to represent the main dynamics of such a system, while easing its tuning owing to its low number of parameters. This facilitates the study of ac-side issues. The key merit of the model is that it allows the representation of the system's behavior with differential equations, which can be used in stability analyses.

Finally, an additional advantage of this simplified model is that the simulation time can be considerably reduced compared to detailed switched models.

The remaining of the paper is structured as follows: Section 2 describes the proposed simplified model; Section 3 compares the results obtained with the proposed model and with a detailed model; finally, the concluding remarks of the paper are provided in Section 5.

2. Model description

The proposed simplified model aims at representing the main dynamics of the dc side of a double-stage FPPT-controlled PV system. To this end, the simplified model has two inputs. The first one is the PV power reference, which is also an input of the real system (see Fig. 2). The second input is the maximum PV power available at each instant (p_{pv}^{max}), which is directly related to the irradiation and the temperature in the real system. The output of the model is the power that would be transferred from the boost converter to the dc-bus capacitor in the real system ($p_{boost\,out}$).

2.1. Simplifying hypotheses

The proposed model is based on a set of simplifying hypotheses:

1. The FPPT dynamics are slow regarding the inner loops of the system (which include the dynamics of the PV voltage control, the boost converter, the inductor L_{boost}, the capacitance C_{pv} and the PV array).
2. The power losses in the boost converter can be approximated by a constant efficiency ratio.
3. For a given PV array and a given temperature, the characteristic curves (p_{pv} vs v_{pv}) are the same for all irradiation levels, provided that p_{pv} is expressed in per unit (pu) for the maximum PV power of each irradiation level.
4. The PV array temperature is kept constant.
5. The PV array works under uniform irradiation conditions.

Hypothesis 1 is very common in controlled systems and allows making two further simplifying assumptions. First, it is assumed that the FPPT dynamics are dominant and, therefore, these are the dynamics that the proposed simplified model tries to reproduce. Second, it is supposed that the steady states of the inductor L_{boost} and the capacitance C_{pv} are rapidly achieved regarding the FPPT dynamics. In other words, it is assumed that the power absorbed or discharged by these two elements will rapidly tend to zero. In consequence, the power going into the boost converter ($p_{boost\,in}$) can be approximated by p_{pv}. Furthermore, if the fluctuations induced by the boost converter switching are neglected, it can be assumed that $p_{boost\,out}$ follows the same behavior as $p_{boost\,in}$. The only difference between these two variables would be caused by the power losses in the boost converter, which, as stated by Hypothesis 2, are modeled with a constant efficiency ratio (η).

On another note, hypotheses 3 and 4 are related to the way the model calculates the initial impact that a p_{pv}^{max} variation has on $p_{boost\,out}$ (i.e., the immediate variation experienced by $p_{boost\,out}$, before the FPPT comes into action). For instance, Fig. 3 illustrates how a PV system would behave after a step decrease in irradiation. In this case, the PV power would experience an immediate change (from p_{pv_a} to p_{pv_b}). This is because the FPPT does not come into play right after a perturbation, and also because the C_{pv} voltage cannot immediately change. Therefore, the value of v_{pv} remains the same right before and after the irradiation change. To calculate the value of p_{pv} after this change, the proposed simplified model assumes that a proportional rule can be applied:

$$p_{pv_b}\left(v_{pv_0}\right) = \frac{p_{pv_a}\left(v_{pv_0}\right)}{p_{pv\ a}^{max}} \times p_{pv\ b}^{max} \iff \frac{p_{pv_b}\left(v_{pv_0}\right)}{p_{pv\ b}^{max}} = \frac{p_{pv_a}\left(v_{pv_0}\right)}{p_{pv\ a}^{max}} \tag{1}$$

It can be noted that (1) is equivalent to supposing that, if p_{pv} is expressed in pu for the maximum PV power, all the characteristic curves of a PV array are equal, independently of the irradiation level. This is precisely what Hypothesis 3 states and it can be proved that this assumption is not far from reality. Fig. 4 shows the characteristic curves of the PV array used in the detailed simulations presented in Section 3. It is observed that all the per-unit curves are very close to each other in most of the PV array operating range. Exceptionally, the low irradiation curves deviate at the right-side of the MPP.

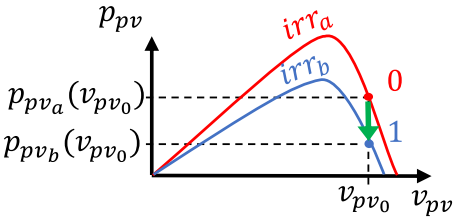

Fig. 3. The immediate consequence of irradiation down a step.

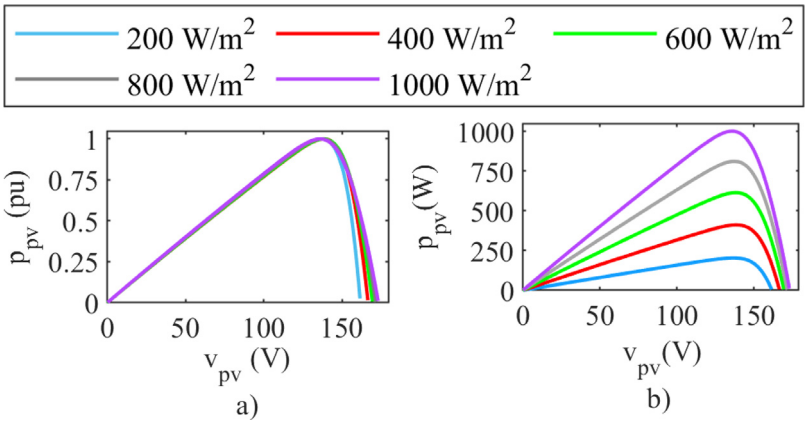

Fig. 4. Characteristic curves of the PV array used for the detailed simulations, for 25 °C. (a) p_{pv} (pu) vs v_{pv} (V). (b) p_{pv} (W) vs v_{pv} (V).

However, it is important to note that the per-unit curves are not equal for different PV array temperatures. This is why Hypothesis 4 has been set. But, once again, this hypothesis is founded on the behavior of real PV arrays. In these, because of cloud passing, the irradiation changes can cause much more significant perturbations than the temperature changes [14,19].

On another note, it is important to stress that the simplified model can only represent irradiation variations of PV arrays subjected to uniform irradiation conditions. This explains Hypothesis 5, a strong assumption necessary for (1) to be accurate. The adaptation of the proposed simplified model to partial shading conditions is a future perspective of this work.

2.2. Model development

The proposed model aims at reproducing the main dynamics of the system's response to perturbations in the PV power reference or irradiation. Whenever there is a change in p_{pv}^{ref}, the FPPT makes v_{pv} vary until the system generates the required PV power. This is represented by Fig. 5(a), where a change from reference a to reference b makes the FPPT move the system from operating point 0 to operating point 1. Therefore, the difference between p_{pv}^{ref} and p_{pv} can be approximated by a delay transfer function. To take into account the energy losses in the boost converter, an efficiency factor (η) can be included. This leads to the simplified model shown in Fig. 6(a).

However, the model of Fig. 6(a) cannot reproduce the system's response to changes in irradiation. Fig. 5(b) depicts how the system would behave in this case. A sudden irradiation reduction would create an immediate change in p_{pv} (represented by the movement from operating point 0 to 1). After that, the FPPT would come into action, and progressively change v_{pv} until p_{pv}^{ref} was reached again (this is represented by the movement from point 1 to point 2).

To reproduce this behavior, the simplified model has been completed, as shown in Fig. 6(b). The main difference with the initial model is that the variable p_{pv}^{ref} divided by p_{pv}^{max} before going through the block that models the FPPT delay and the boost converter losses. This is equivalent to expressing p_{pv}^{ref} in per unit. The resulting variable is multiplied again by p_{pv}^{max} to undo the per-unit conversion. Finally, it is observed that $p_{pv}{}_{pu}^{ref}$ also goes through

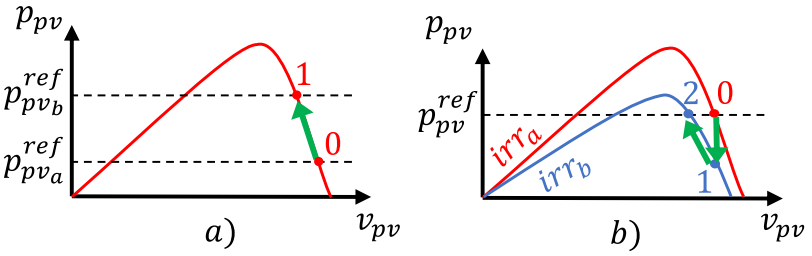

Fig. 5. The behavior of an FPPT-controlled PV array in response to: (a) a change in p_{pv}^{ref}, (b) a change in irradiation.

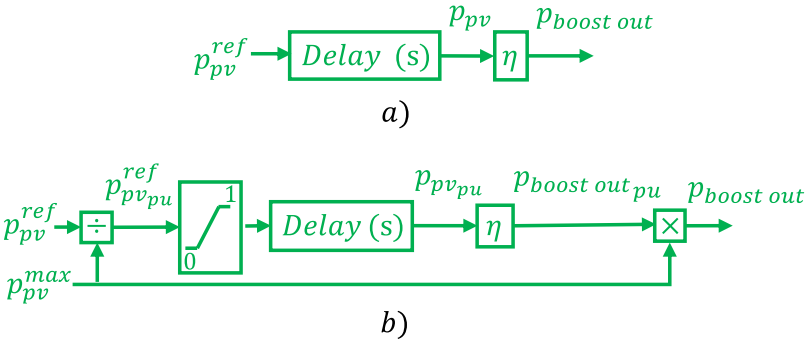

Fig. 6. Proposed simplified models. (a) Partial. (b) Complete.

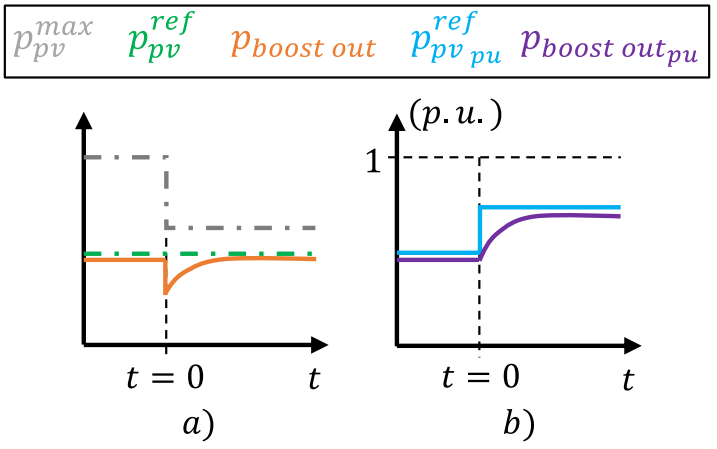

Fig. 7. Evolution of the simplified model under a step change of p_{pv}^{max}.

a saturation block, which models the physical limits of the system (i.e., the fact that the PV power will never be negative or greater than the maximum available power).

The importance of this new model feature can be understood by picturing a scenario in which p_{pv}^{max} experiences a step change, while p_{pv}^{ref} is kept constant. Because $p_{boost\ out}$ is the direct product of $p_{boost\ out\ pu}$ and p_{pv}^{max}, the step change of this last variable causes an immediate step in $p_{boost\ out}$. It models the initial change experienced by $p_{boost\ out}$ when an irradiation change occurs, before the FPPT comes into action. The subsequent action of the FPPT is also modeled. The input step of p_{pv}^{max} also causes an immediate step in $p_{pv\ pu}^{ref}$. However, thanks to the delay, this step is only progressively reflected on $p_{boost\ out}$, and this reproduces the FPPT response. Fig. 7 presents how the simplified model variables would evolve in this scenario.

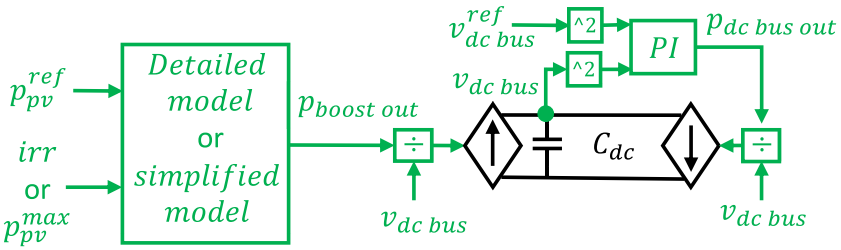

Fig. 8. Outer simulation model structure.

3. Simulation results

This section presents a comparison of the simulation results obtained with a detailed model of an FPPT-controlled PV system and with the proposed simplified model. To facilitate the comparison of the results, the same outer structure has been used with both simulation models, shown in Fig. 8, where the controlled current sources can be considered ideal current sources that perfectly follow the provided reference.

As already explained, the output of the detailed model and the simplified model coincide ($p_{boost\ out}$). However, it is not easy to compare both outputs because, in the detailed model, $p_{boost\ out}$ is highly distorted by the peaks caused by the boost converter switching. To solve this issue, a dc bus capacitor has been added to the simulation, so that the dc bus voltage ($v_{dc\,bus}$) can be compared in the detailed and in the simplified simulation. Since the capacitor naturally filters the high-frequency oscillations, $v_{dc\,bus}$ will be mostly affected by the slower dynamics of the system (i.e., the dynamics caused by the FPPT reaction to changes in p_{pv}^{ref} and in the irradiation). These are precisely the dynamics that the simplified model wants to reproduce. Therefore, $v_{dc\,bus}$ is an appropriate magnitude to evaluate the performance of this model. In addition, it is a key magnitude in real systems, because its behavior directly affects the inverter and, in consequence, the ac-side stability. Finally, to complete the outer model structure, a proportional–integral regulator has been added. This regulator ensures the stability of $v_{dc\,bus}$ by commanding the power that goes out of the dc bus ($p_{dc\,bus\,out}$).

It should be noted that both the detailed and the simplified simulation models have been implemented using MATLAB/Simulink. Sections 3.1 and 3.2 provide more details on their tuning.

3.1. Detailed model tuning

Regarding the detailed model, the FPPT proposed by [18] has been implemented. It relies on the perturb-and-observe (P&O) principle: with a fixed periodicity, the algorithm imposes a positive or negative step to v_{pv}, and observes if this makes p_{pv} get closer to p_{pv}^{ref} or further away from it. This result is used by the algorithm to decide the direction of the voltage step for the next iteration. Besides this general working principle, the specificity of the chosen FPPT algorithm is that it is capable of detecting if the system is in transient or in steady state operation, and adapting the amplitude of the voltage step accordingly. Another key feature of the selected FPPT strategy is its capacity to detect whether a variation in p_{pv} has been caused by an imposed voltage step or by external irradiation or temperature variation. This allows the algorithm to reduce the number of mistakes when deciding the direction of the voltage step for the next FPPT iteration. Finally, this FPPT allows the system to operate both on the right and the left sides of the MPP. It is important to emphasize that the simplified model has been tuned and tested for both operation sides. However, since both cases give similar results, only the curves corresponding to the right-side operation are plotted in Section 3.3.

On another note, the PV voltage regulator block has been implemented using the control structure proposed by [12]. It relies on a model predictive control strategy and makes v_{pv} fastly converge towards its reference.

Finally, a switched model has been used for the boost converter and a one-diode model has been implemented for the PV array. The PV characteristic curves are shown in Fig. 4, while the rest of the model parameters are summarized in Table 1.

Table 1
Detailed and simplified model parameters.

Dc bus		
$v_{dc\,bus}^{nom}$	185 V	
$C_{dc\,bus}$	7.5 mF	
$v_{dc\,bus}$ regulator - k_p	0.15 W/V^2	
$v_{dc\,bus}$ regulator - k_i	1.5 W/V^2/s	
Detailed model		
Physical components		
Nominal power	1000 W	
L_{boost}	2 mH	
C_{pv}	0.51 mF	
Boost converter $f_{switching}$	25 kHz	
FPPT	Left-side op.	Right-side op.
T_{step}	5 ms	5 ms
V_{step-b}	3.0 V	1.8 V
$V_{step\,min}$	0.60 V	0.36 V
k_1	1.22 e-1	1.85 e-2
k_2	2.25 e-2	7.84 e-3
dp threshold	50 W	50 W
dp/dv threshold	3.8 W/V	0.77 W/V
Simplified model		
	Left-side op.	Right-side op.
Delay time constant	39 ms	24 ms
η	96%	98%

3.2. Simplified model tuning

First, to shape the delay transfer function of the simplified model, the detailed model has been run several times. It has been observed that, for the FPPT proposed by [18], the delay between p_{pv}^{ref} and p_{pv} can be approximated by a first-order transfer function. And, although the delay time constant varies somewhat depending on the operating point of the PV array, it has been decided to use a unique delay transfer function with an average time constant. Second, to tune the efficiency ratio η, the boost converter losses have been analyzed for multiple operating points of the PV system. Typical efficiency values (in the range from 95% to 98%) have been observed.

The resulting parameters of the simplified model are also presented in Table 1. Note that no correlations were considered between parameters of the simplified model and the real FPPT as the objective is not to match accurately a particular FPPT, but rather dispose of a model that captures dynamics that need reproducing in upcoming stability studies.

3.3. Simulation results comparison

The main simulation results are presented and analyzed hereafter. For each simulated scenario, the variables $v_{dc\,bus}$ and p_{pv} are plotted for both the detailed model (*det.*) and the simplified model (*simpl.*).

The first scenario consists of keeping constant irradiation (or p_{pv}^{max}), while imposing step increments and decrements to p_{pv}^{ref}. The results of this simulation are depicted in Fig. 9. As anticipated, the behavior of p_{pv} is properly reproduced with a first-order delay. Furthermore, the average time constant provides accurate results for most of the simulated steps. In consequence, $simpl.v_{dc\,bus}$ matches $det.v_{dc\,bus}$ correctly. Therefore, the first-order delay block of the simplified model is validated.

Fig. 10 presents, in turn, the results of a scenario in which p_{pv}^{ref} is kept constant and the irradiation experiences step changes. For most of the simulated steps, the simplified model manages to provide an accurate estimation of the initial fluctuation experienced by $p_{boost\,out}$ after an irradiation change. Note that this is the case even for FPPT right-side operation, for which Hypothesis 3 is less realistic.

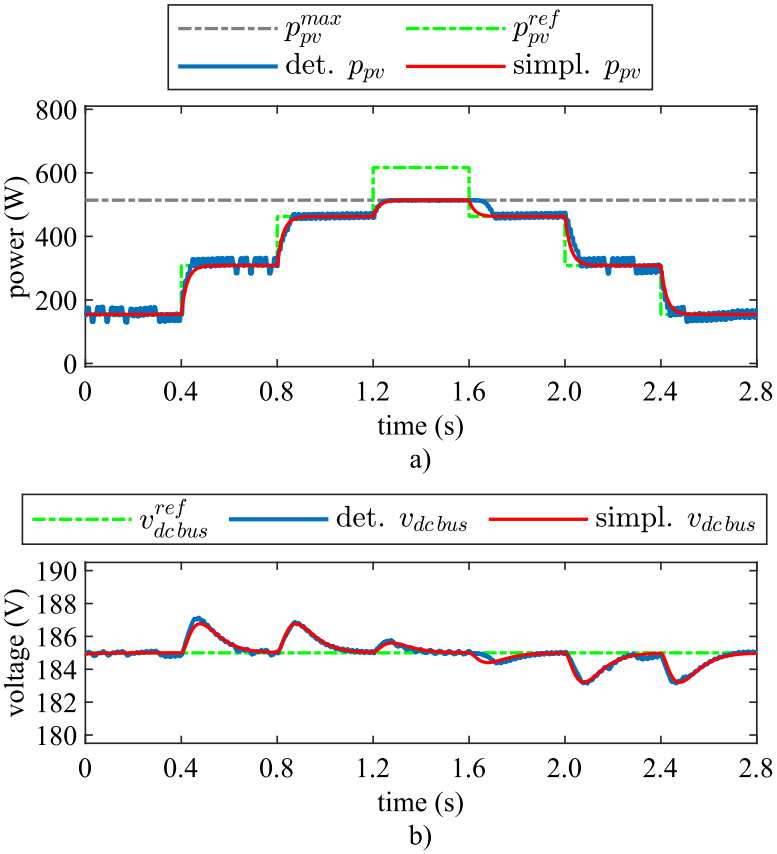

Fig. 9. Response of the detailed and simplified models to p_{pv}^{ref} steps, for FPPT right-side operation. (a) Voltage curves. (b) Power curves.

Nevertheless, it may seem that the simplified model is not very accurate in some cases (at $t = 0.4$ s and $t = 0.8$ s). But, as shown in the magnified portion of Fig. 10, this is not due to a wrong estimation of the initial fluctuation of $p_{boost\,out}$. Because the irradiation variations are so fast, the FPPT of the detailed model is not able to detect them properly and, in consequence, it chooses the wrong v_{pv} step for the following iteration. This causes p_{pv} to move in the wrong direction for one FPPT iteration. This occasional FPPT malfunctioning cannot be reflected by the simplified model. However, it is important to note that the FPPT proposed by [18] would be able to avoid this malfunction in a real life scenario, because the irradiation changes would not be so abrupt. It can then be concluded that the second branch of the simplified simulation model is valid (i.e., the branch dividing and multiplying by p_{pv}^{max}, which is directly responsible for the variations of $p_{boost\,out}$ after a change in p_{pv}^{max}).

Finally, another detail that may be remarked in Fig. 10(a) is that, at $t = 1.2\,s$, there is not a first-order response following the step decrease in p_{pv}. In the detailed simulation, this happens because, right before $t = 1.2$ s, the system is already operating at the MPP. Then, after the irradiation decrease occurs, the FPPT barely has to change v_{pv} to reach the MPP again. In consequence, the first-order response is not observed. Regarding the simplified model, this behavior is reproduced using the saturation block. Before the irradiation decrease, ${p_{pv}}_{pu}^{ref}$ has already reached its upper limit. This explains why, when p_{pv}^{max} decreases, the output of the saturation block does not change and, in consequence, the first-order delay is not triggered.

4. Application to small-signal stability study

4.1. State–space formulation

The proposed simplified model reveals the main dynamics of the dc side of double-stage FPPT-controlled PV systems. Its formulation with differential equations is adapted to stability studies. The simplified model can be

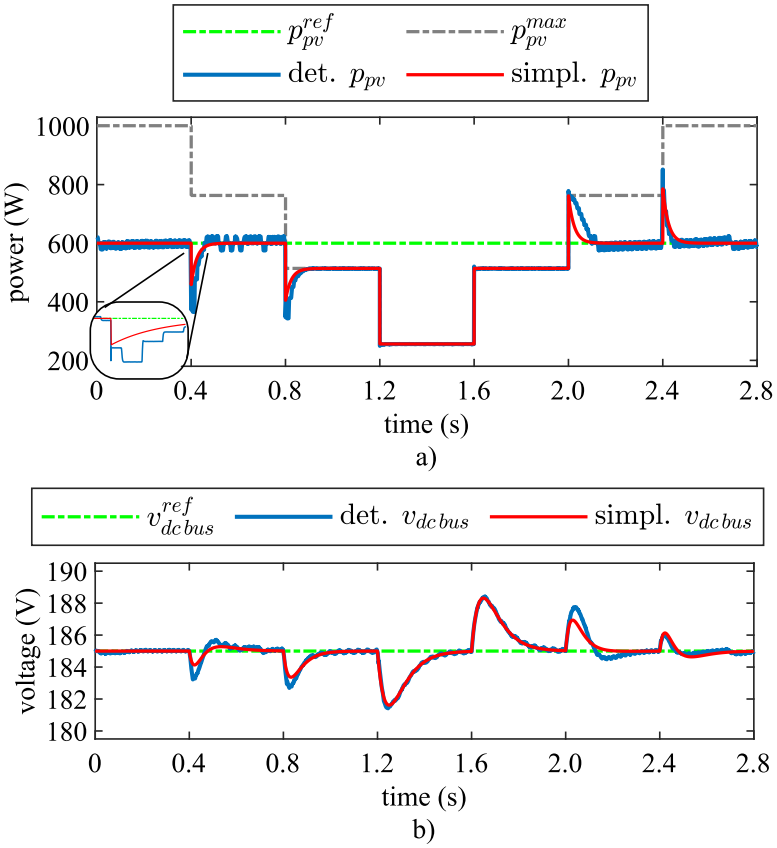

Fig. 10. Response of the detailed and simplified models to p_{pv}^{max} steps, for FPPT right-side operation. (a) Voltage curves. (b) Power curves.

translated into three state–space formulations, where $p_{pv_{pu}}$ is the state variable, p_{pv}^{max} and p_{pv}^{ref} are the inputs, and $p_{boost\,out}$ is the output. As in Section 3, the delay of the proposed model is represented with a first-order transfer function of time constant τ.

Part 1: If $p_{pv_{pu}}^{ref}$ stays between 0 and 1, the saturation of the proposed simplified model is not active. This leads to the state–space formulation of (2).

Part 2: When $p_{pv_{pu}}^{ref}$ saturates at 1 and the output of the delay reaches the steady state, the dynamic introduced by this delay is "wiped out" (canceled). This leads to the state–space formulation (3), in which $p_{pv_{pu}}$ and $p_{boost\,out}$ are held constant.

Part 3: When $p_{pv_{pu}}^{ref}$ saturates at 0 and the output of the delay reaches the steady state, then the dynamic introduced by this delay is "wiped out" (canceled). This leads to the state–space formulation (4), in which $p_{pv_{pu}}$ and $p_{boost\,out}$ are held constant.

$$\text{Part 1:} \begin{cases} \dot{p_{pv_{pu}}}(t) & = \dfrac{1}{\tau} \times \dfrac{p_{pv}^{ref}(t)}{p_{pv}^{max}(t)} - \dfrac{1}{\tau} \times p_{pv_{pu}}(t) \\ p_{boost\,out}(t) & = \eta \times p_{pv_{pu}}(t) \times p_{pv}^{max}(t) \end{cases} \tag{2}$$

$$\text{Part 2:} \begin{cases} \dot{p_{pv_{pu}}}(t) & = 0 \\ p_{boost\,out}(t) & = \eta \times p_{pv}^{max}(t) \end{cases} \tag{3}$$

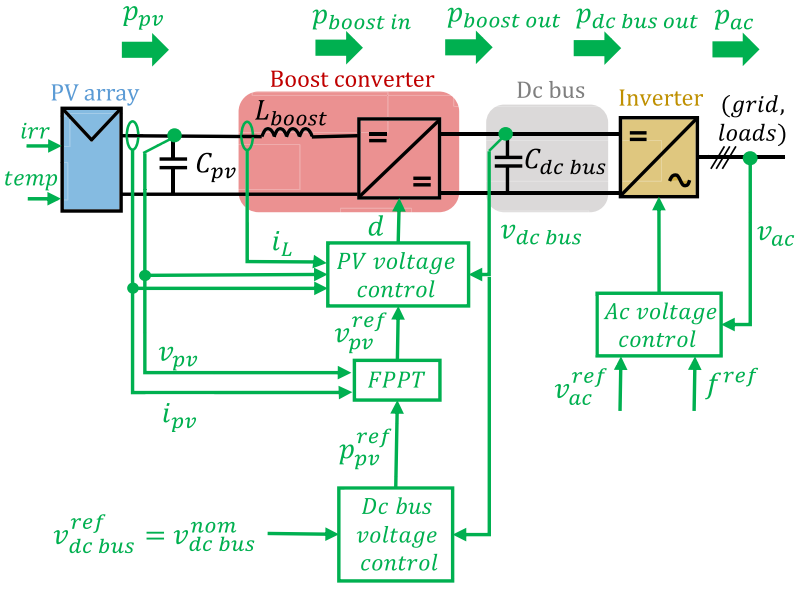

Fig. 11. Variables definition for the grid-forming control of a double-stage FPPT-controlled PV system and power transfers.

$$\text{Part 3:} \begin{cases} \dot{p_{pv}}_{pu}(t) & = 0 \\ p_{boost\ out}(t) & = 0 \end{cases} \tag{4}$$

These three state–space formulations help evaluate how the dc side dynamics affect the stability of a double stage FPPT-controlled PV system, notably in the case of a grid-forming control, as depicted in Fig. 11. In grid-forming systems, the inverter is controlled to impose a constant voltage and frequency on its ac side, while the power it delivers (p_{ac}) constantly adapts to the power absorbed by the ac loads. In consequence, the power going out of the dc bus ($p_{dc\ bus\ out}$, which can be approximated to p_{ac} if the inverter losses are neglected), also changes as the power absorbed by the ac loads change. To ensure that the dc bus voltage remains constant, the dc bus voltage control updates p_{pv}^{ref} and transfers it to the FPPT.

4.2. Small signal stability

4.2.1. Typical conditions

To undertake a stability analysis for such system, we combine (2) with the differential equations describing the dynamics of the dc bus capacitor and the regulator. This leads to the state–space formulation (5), in which the dc bus voltage control is a proportional integral controller of parameters k_p and k_i. In this formulation v_{dc}, ϕ and $p_{pv\,pu}$ are the state variables, p_{pv}^{max} and $p_{dc\ bus\ out}$ are the inputs. Note that ϕ models the dynamics of the integral part of the $v_{dc\ bus}$ regulator.

$$\begin{cases} \dot{v_{dc}}(t) & = \dfrac{1}{C_{dc\ bus}} \times \dfrac{\eta \times p_{pv\,pu}(t) \times p_{pv}^{max}(t) - p_{dc\ bus\ out}(t)}{v_{dc}(t)} \\ \dot{\phi}(t) & = k_i \times \left(v_{dc}^{nom\,2} - v_{dc}(t)^2\right) \\ \dot{p_{pv}}_{pu}(t) & = \dfrac{1}{\tau} \times \dfrac{k_p \times \left(v_{dc}^{nom\,2} - v_{dc}(t)^2\right) + \phi(t)}{p_{pv}^{max}(t)} - \dfrac{1}{\tau} \times p_{pv\,pu}(t) \end{cases} \tag{5}$$

After the linearization of the state–space formulation (5) around an operating point (the linearized equations have been omitted for brevity), the small-signal analysis and participation theory [16] allow computing the poles of the system. In this paper, we study how they evolve as k_p and k_i change.

The system parameters used in the stability analysis are synthesized in Table 2. It can be observed that the detailed model uses the same FPPT as in Section 3. However, the time constant of the equivalent simplified model

Table 2
Parameters used for the stability analysis.

Dc bus	
$v_{dc\,bus}^{nom}$	185 V
$C_{dc\,bus}$	7.5 mF
Detailed model	
Physical components	
Nominal power	1000 W
L_{boost}	2 mH
C_{pv}	0.51 mF
Boost converter $f_{switching}$	25 kHz
FPPT	Right-side op.
T_{step}	5 ms
V_{step-b}	1.8 V
$V_{step\,min}$	0.36 V
k_1	1.85 e-2
k_2	7.84 e-3
dp threshold	50 W
dp/dv threshold	0.77 W/V
Simplified model	
	Right-side op.
Delay time constant	15 ms
η	98%
Operating point for linearization	
p_{pv}^{max}	907 W
$p_{dc\,bus\,out}$	400 W

Table 3
Poles of the system for $k_p = 0.06\,\mathrm{W/V^2}$ and $k_i = 0.36\,\mathrm{W/V^2/s}$ (typical conditions).

Eigenvalues			
	λ_1	λ_2	λ_3
	$-9.63 - 6.29i$	$-9.63 - 6.29i$	-47.4
Participation matrix (modules)			
	λ_1	λ_2	λ_3
$v_{dc\,bus}(t)$	1.37	1.37	0.62
$\phi(t)$	1.13	1.13	0.09
$p_{pv}^{pu}(t)$	0.27	0.27	1.53

is different, because, to obtain a precise stability analysis, we refined this time constant for the simplified model to better match the detailed model around the selected operating point (in Section 3, the time constant was obtained averaging the detailed model's FPPT delay at various operating points).

Table 3 displays the poles of the system for $k_p = 0.06\,\mathrm{W/V^2}$ and $k_i = 0.36\,\mathrm{W/V^2/s}$. It also displays the participation factors, which measure the net participation of each pole in the dynamic of each state variable, and vice-versa. The system contains a fast pole with no imaginary part (λ_3), which is mostly associated with the state variable $p_{pv_{pu}}$ (i.e., to the FPPT delay). There are also two complex conjugate poles, which are mostly associated with the dynamics of v_{dc} (i.e., the capacitor) and ϕ (the integrator).

To ensure that these poles correctly describe the dynamics of the analyzed system, we can simulate its response to an input change using the detailed model, and the linearized state–space formulation derived from the simplified model. Fig. 12 shows that both simulations match, which confirms the accuracy of the stability analysis.

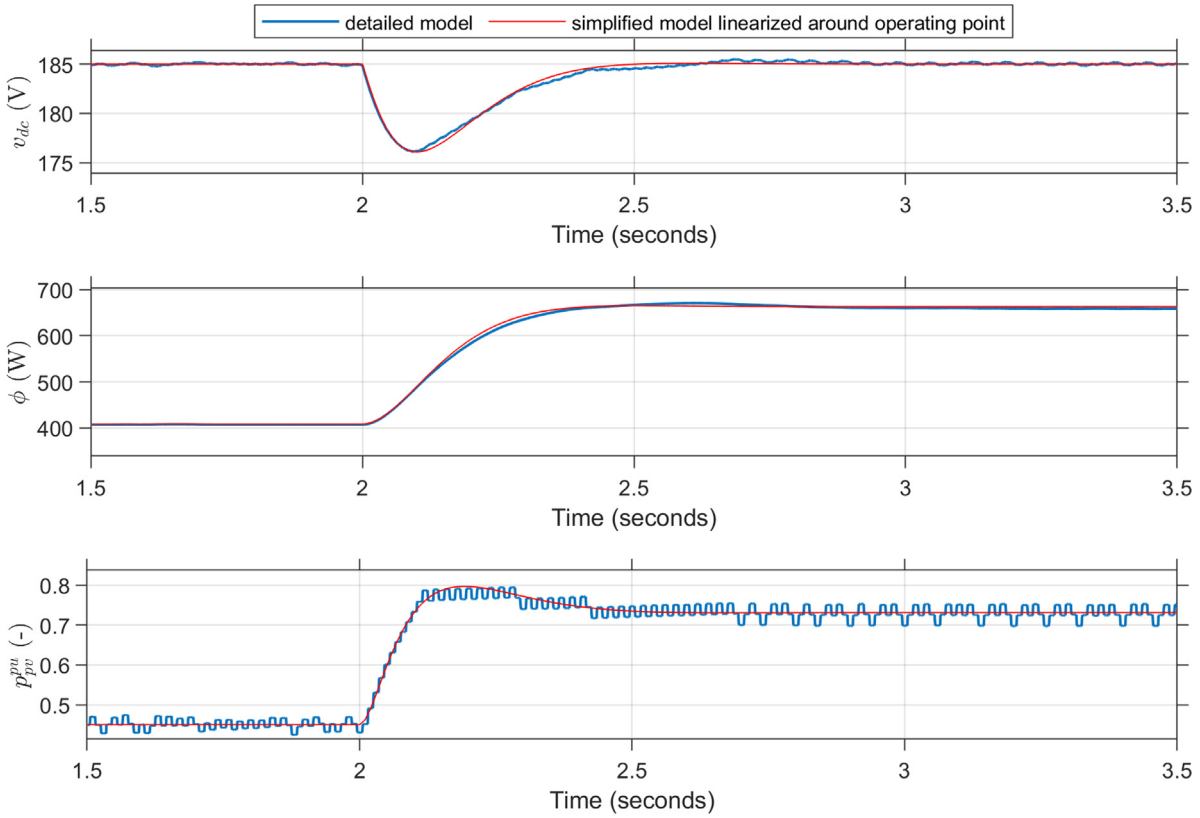

Fig. 12. Response to an input change of the detailed model (in blue), and the linearized state–space formulation derived from the simplified model (in red) of the grid-forming control of the double-stage FPPT-controlled PV in typical conditions. (For interpretation of the references to color in this figure legend, the reader is referred to the web version of this article.)

Table 4
Poles of the system for $k_p = 0.06\,\mathrm{W/V^2}$ and $k_i = 1.8\,\mathrm{W/V^2/s}$ (constrained conditions).

Eigenvalues			
	λ_1	λ_2	λ_3
	$-4.35 - 22.8i$	$-4.35 - 22.8i$	-58
Participation matrix (modules)			
	λ_1	λ_2	λ_3
$v_{dc\,bus}(t)$	0.58	0.58	0.15
$\phi(t)$	0.51	0.51	0.16
$p_{pv}^{pu}(t)$	0.20	0.20	0.99

4.2.2. Constrained conditions

We can also study what happens if we use a much more aggressive regulator, by multiplying k_i by 5. The poles and of the system are displayed in Table 4. The imaginary part of the two complex conjugate poles has considerably increased, which indicates that the system will present much less damped oscillations. In addition, we can observe that the relative participation of $p_{pv\,pu}$ in these poles has increased (i.e., the participation of v_{dc} and ϕ is divided by two, while that of $p_{pv\,pu}$ stays similar). This indicates a stronger influence of the FPPT delay on the oscillations.

Once again, the accuracy of the stability analysis is validated through simulations, as shown in Fig. 13.

The stability analysis has delivered very accurate results because the delay constant of the simplified model has been selected for the specific operating point analyzed. To ensure the suitability of the dc bus voltage control in

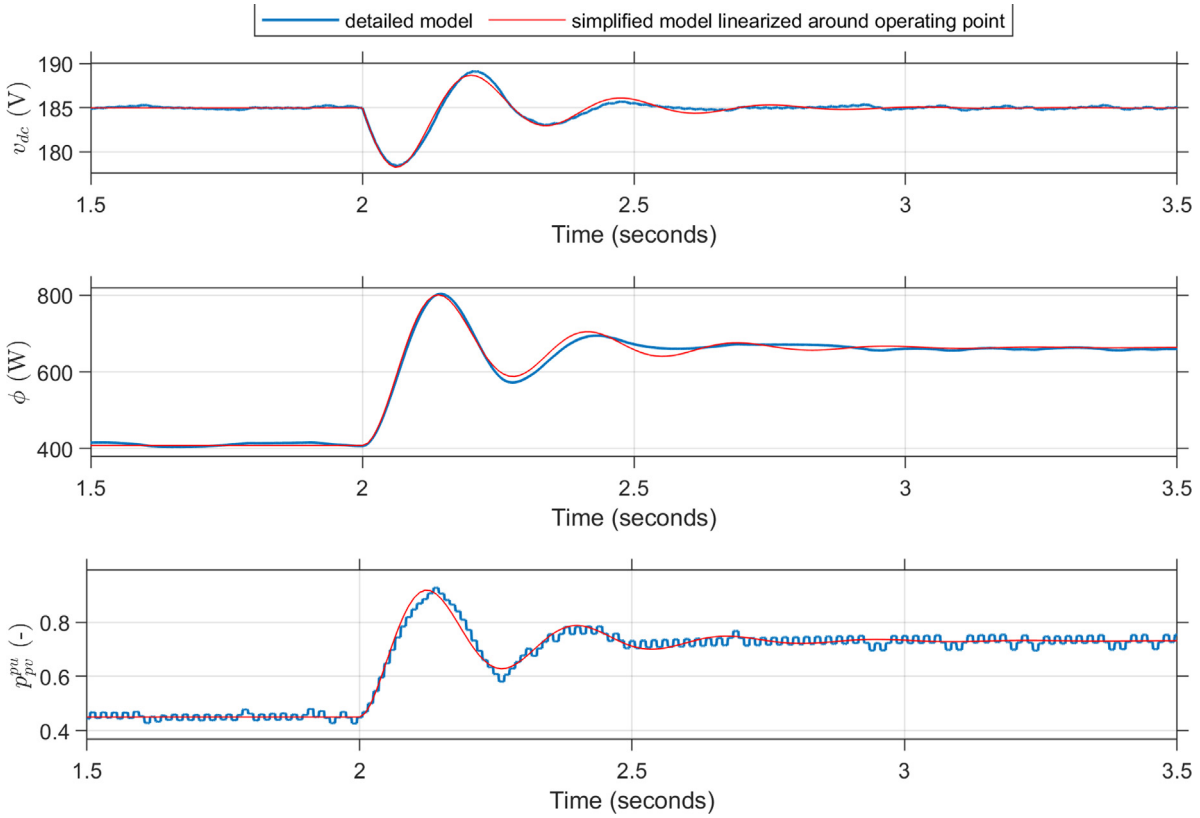

Fig. 13. Response to an input change of the detailed model (in blue), and the linearized state–space formulation derived from the simplified model (in red) of the grid-forming control of the double-stage FPPT-controlled PV in more constrained conditions. (For interpretation of the references to color in this figure legend, the reader is referred to the web version of this article.)

all operating points, the analysis should be undertaken in the worst-case scenario (i.e., the operating point in which the greatest FPPT delay is observed in the detailed model).

5. Discussions and conclusions

The proposed simplified model captures the main dynamics of the dc side of an FPPT-controlled double-stage PV unit. This model is based on a set of simplifying hypotheses, most of which are coherent with the behavior and operating conditions of a real system. The only strong hypothesis supposes that the PV array is subjected to uniform irradiation conditions. The adaptation of the proposed model to partial shading conditions is a future perspective of this work.

To build the simplified model, it is necessary to approximate the delay of the FPPT by a transfer function. The FPPT proposed by [18] is specially adapted for this, but a potential perspective of this work is to find appropriate transfer functions for other FPPTs, and in particular for those based on nonlinear search algorithms such as [5,7]. In addition to the transfer function, the proposed model relies on a mechanism to calculate the instantaneous impact of an irradiation change on p_{pv}. The adequacy of this mechanism has been illustrated using temporal simulations. The results of the simplified model would be even more accurate under more realistic scenarios, with ramp irradiation changes instead of step variations.

Naturally, the precision of the simplified dc side depends on the precision of the transfer function approximation. However, the key advantage of the proposed model is not the ability to accurately match the response of a particular FPPT. This would be very challenging with such a simplified model since, as illustrated in the article, an FPPT response can vary from one PV array operating point to another. The main advantage of the proposed simplified model is that, with a very simple and linearizable architecture, it can reproduce the typical response of the system

to both changes in the PV power reference and the irradiation (two perturbations very different in nature). This is useful to:

- Reduce the computational burden and modeling efforts when simulating ac grids with one or several double-stage FPPT-controlled PV systems, since the complex and nonlinear FPPT algorithms and v_{pv} regulators are avoided.
- Introduce the dc side of double-stage FPPT-controlled PV systems in stability studies. This development is of major importance since many FPPT algorithms cannot be directly expressed in a differential form (like P&O-based FPPTs, which use decision trees).

In both cases, the transfer function modeling the FPPT delay can be tuned concerning the worst-case scenario (i.e., the PV array operating point where the FPPT response is slowest or the least damped). Alternatively, this transfer function can be tuned arbitrarily and varied to obtain the limit tuning that allows proper and stable functioning of the system.

Acknowledgments

This work has been funded in the scope of the NTU – CNRS "Excellence Science" Joint Research Program.

References

[1] Technical regulation 3.2.2 for PV power plants above 11 kW, Energinet, Denmark, Document No.: 14/17997-39, 2016.
[2] Procedures for monitoring the performance of Generation Facilities connected to the Public Distribution Network managed by Enedis, (in French), Enedis, France, Document No: Enedis-PRO-RES_64E, 2020.
[3] L.V. Bellinaso, H.H. Figueira, M.F. Basquera, R.P. Vieira, H.A. Gründling, L. Michels, Cascade control with adaptive voltage controller applied to photovoltaic boost converters, IEEE Trans. Ind. Appl. 55 (2) (2019) 1903–1912.
[4] Z. Chen, R.H. Lasseter, T.M. Jahns, Active power reserve control for grid-forming PV sources in microgrids using model-based maximum power point estimation, in: Proc. ECCE, 2019.
[5] R. Gomez-Merchan, S. Vazquez, A. Marquez Alcaide, H. Dehghani Tafti, J.I. Leon, J. Pou, C.A. Rojas, S. Kouro, L.G. Franquelo, Binary search-based flexible power point tracking algorithm for photovoltaic systems, IEEE Trans. Ind. Electron. 68 (7) (2021) 5909–5920.
[6] R.S. Kenney, Electric rule no.21 generating facility interconnections, in: PG & E, San Francisco, CA, USA, 2018.
[7] A. Kumaresan, H.D. Tafti, N.K. Kandasamy, G.G. Farivar, J. Pou, T. Subbaiyan, Flexible power point tracking for solar photovoltaic systems using secant method, IEEE Trans. Power Electron. 36 (8) (2021) 9419–9429.
[8] Z. Li, K.W. Chan, J. Hu, J.M. Guerrero, Adaptive droop control using adaptive virtual impedance for microgrids with variable PV outputs and load demands, IEEE Trans. Ind. Electron. 68 (10) (2021) 9630–9640.
[9] H. Liu, Y. Yang, X. Wang, P.C. Loh, F. Blaabjerg, W. Wang, D. Xu, An enhanced dual droop control scheme for resilient active power sharing among paralleled two-stage converters, IEEE Trans. Power Electron. 32 (8) (2017) 6091–6104.
[10] H. Mahmood, J. Jiang, Decentralized power management of multiple PV, battery, and droop units in an islanded microgrid, IEEE Trans. Smart Grid 10 (2) (2019) 1898–1906.
[11] J. Matevosyan, B. Badrzadeh, T. Prevost, E. Quitmann, D. Ramasubramanian, H. Urdal, S. Achilles, J. MacDowell, S.H. Huang, V. Vital, J. O'Sullivan, R. Quint, Grid-forming inverters: Are they the key for high renewable penetration?, IEEE Power Energy Mag. 17 (6) (2019) 89–98.
[12] A. Narang, H.D. Tafti, C.D. Townsend, G.G. Farivar, J. Pou, G. Konstantinou, S. Vazquez, An algorithm for fast flexible power point tracking in photovoltaic power plants, in: Proc. IECON, 2019, pp. 4387–4392.
[13] V.D. Paduani, H. Yu, B. Xu, N. Lu, A unified power-setpoint tracking algorithm for utility-scale PV systems with power reserves and fast frequency response capabilities, IEEE Trans. Sust. En. 13 (1) (2022) 479–490.
[14] B. Pawar, S. Chakrabarti, E.I. Batzelis, B.C. Pal, Grid-forming control for solar PV systems with real-time MPP estimation, in: 2021 IEEE Power & Energy Society General Meeting, PESGM, 2021.
[15] Q. Peng, A. Sangwongwanich, Y. Yang, F. Blaabjerg, Grid-friendly power control for smart photovoltaic systems, Sol. Energy 210 (2020) 115–127.
[16] L. Rouco, F.L. Pagola, G.C. Verghese, I.J. Pérez-Arriaga, Selective modal analysis, in: Power System Coherency and Model Reduction, first ed., Springer, New York, 2013, pp. 199–258.
[17] H.D. Tafti, G. Konstantinou, C.D. Townsend, G.G. Farivar, A. Sangwongwanich, Y. Yang, J. Pou, F. Blaabjerg, Extended functionalities of photovoltaic systems with flexible power point tracking: Recent advances, IEEE Trans. Power Electron. 35 (9) (2020) 9342–9356.
[18] H.D. Tafti, A. Sangwongwanich, Y. Yang, J. Pou, G. Konstantinou, F. Blaabjerg, An adaptive control scheme for flexible power point tracking in photovoltaic systems, IEEE Trans. Power Electron. 34 (6) (2019) 5451–5463.
[19] W. Xiao, W.G. Dunford, P.R. Palmer, A. Capel, Regulation of photovoltaic voltage, IEEE Trans. Ind. Electron. 54 (3) (2007) 1365–1374.